

# CHAPTER 3

---

## Instrument Descriptions

**Lead Authors:**

Patrick Hamill  
Colette Brogniez  
Larry Thomason  
Terry Deshler

**Authors:**

Juan Carlos Antuña  
Darrel Baumgardner  
Richard Bevilacqua  
Charles A. Brock  
Christine David  
Michael Fromm  
Didier Fussen  
Mark Hervig  
Chris A. Hostettler  
Shan-Hu Lee  
John Mergenthaler  
Mary T. Osborn  
Graciela B. Raga  
J. Michael Reeves  
James Rosen  
James C. Wilson

**Contributors:**

Sharon P. Burton  
Nina Iyer



### 3.1 Introduction

The properties of stratospheric aerosol particles are measured with various types of instrument. Each instrument measures a particular subset of aerosol properties. None provides a complete depiction of aerosol composition and size distribution. Consequently, measurements from different instruments are often not directly comparable and the values of aerosol properties indirectly inferred from the base measurements may not always be consistent. In this chapter we provide brief descriptions of the instruments to assist the reader in interpreting the measured values and the inferred aerosol properties, as well as to understand instrument characteristics and limitations. The results obtained and the aerosol properties inferred from these measurements are presented in Chapter 4.

Measurements of the stratospheric aerosol can be characterized in the following manner:

- “global long term measurements” (Section 3.2),
- “global short term measurements” (Section 3.3),
- “localized long term measurements” (Section 3.4), and
- “localized short term measurements” (Section 3.5).

The term “global” is used loosely and is intended to convey the idea that the measurements cover a large geographic region. Therefore the POAM measurements are classified as “global” even though they only cover the Arctic and Antarctic regions. The CLAES data cover a much larger region of the Earth, but the experiment had a (planned) lifetime of only 19 months, so it is classified as “global short term.” Measurements made from a fixed location, such as lidar measurements, which have been carried out routinely for a long period of time are classified as “localized long term measurements.” Measurements made with instruments mounted on aircraft are classified as “localized short term measurements.” While this document is primarily focused on long-term global measurements, shorter term and more spatially isolated data sets are relevant because they also contribute significantly to the body of information on the stratospheric aerosol. In addition, they provide key validation for the other data sets, and they are useful for filling in the gaps in the global long-term data sets.

The data presented in this assessment are representative but not comprehensive. There are a number of very valuable data sets that for one reason or another were not included in this report. Among them are the stratospheric aerosol data sets obtained by the Solar Mesosphere Explorer (SME) satellite [Rusch et al., 1994; Eparvier et al., 1994], ILAS and ILAS II, the Improved Limb Atmospheric Spectrometer [Sasano, 2002], the Improved Stratospheric and Mesospheric Sounder (ISAMS) on the Upper Atmosphere Research Satellite [Lambert et al., 1993], the balloon-borne mass spectrometer of the Max Planck Institute [Weisser, et al., 2005] and data from several lidar stations.

### 3.2 Global Long-Term Measurements

The measurement systems discussed below have dissimilar coverage both in space and time. In Table 3.1 we present the coverage for instruments having global or large geographic area coverage. See the appropriate sections for the coverage of instruments with limited geographic coverage.

**Table 3.1: Geographic and Temporal Coverage by “Global Scale” Instruments**

<b>Instrument</b>	<b>Geographic Coverage</b>	<b>Time Frame</b>
SAM II	64-83 S and 64-83 N	Oct 1978-Dec 1993
SAGE I	80 S - 80 N	Feb 1979 - Nov 1981
SAGE II	80 S - 80 N	Oct 1984 - present
HALOE	80 S to 80 N	October 1991 - present
POAM II	63-88 S and 54-71 N	Sept 1993 - Nov 1996
POAM III	63-88 S and 54-71 N	March 1998 - present
CLAES	34N to 80S or 34S to 80N	Oct 1991 - May 1993
ORA	40 S – 40 N	Aug 1992 – May 1993

### 3.2.1 SAM II, SAGE I, and SAGE II: The Occultation Technique

The Stratospheric Aerosol and Gas Experiment (SAGE) is a series of NASA instruments that have produced global measurements of stratospheric aerosol extinction in the visible and near infrared since 1978. This series consists of the Stratospheric Aerosol Measurement (SAM II) (1978-1993), SAGE (1979-1981), SAGE II (1984-present), and the more recently launched SAGE III. Although SAGE could be considered “short term” we have included it here as it is one of a series of similar instruments. These instruments provide from one to nine wavelengths of aerosol extinction measurements, and yield an unbroken record of aerosol extinction at 1000 nm that extends from 1978 through the present. Data from these instruments have been extensively used in international assessments of changes to stratospheric ozone and water vapor [WMO, 2003, SPARC, 2000] as well as being previously used in the evaluation of stratospheric aerosol trends [Thomason et al., 1997a; Bauman et al., 2003a,b; Bingen et al., 2004a,b] and the creation of aerosol products useful in models of chemical/dynamical processes such as aerosol surface area density [Thomason et al., 1997b].

The SAGE series of instruments use the solar occultation technique to measure atmospheric transmission along the line of sight between the spacecraft and the Sun along paths passing through the atmosphere. Consequently, the Sun, relative to the instrument, is being occulted or obscured by the atmosphere and the solid Earth. The geometry is shown in Figure 3.1. This is a common measurement strategy for space-based instruments focused primarily on the stratosphere and is used by the Halogen Occultation Experiment (HALOE) and the Polar Ozone and Aerosol Measurement (POAM). It is well suited for situations in which horizontal inhomogeneity is not a significant concern and where the optical depth is relatively low: features that are generally characteristic of the stratosphere. In applying the technique, each spherical layer of the atmosphere is assumed to be homogeneous. For layers 1 km thick, an onion peeling technique extending from 10 km to 40 km, would require horizontal homogeneity over a line of sight of about 1200 km. For a smaller altitude range or thicker layers, the homogeneity requirement is less restrictive, but it should be kept in mind that this is an inherent assumption in the technique.

An event, defined as a set of the measurement of line-of-sight transmission at different tangential altitudes, occurs during each sunrise or sunset encountered by the spacecraft. This

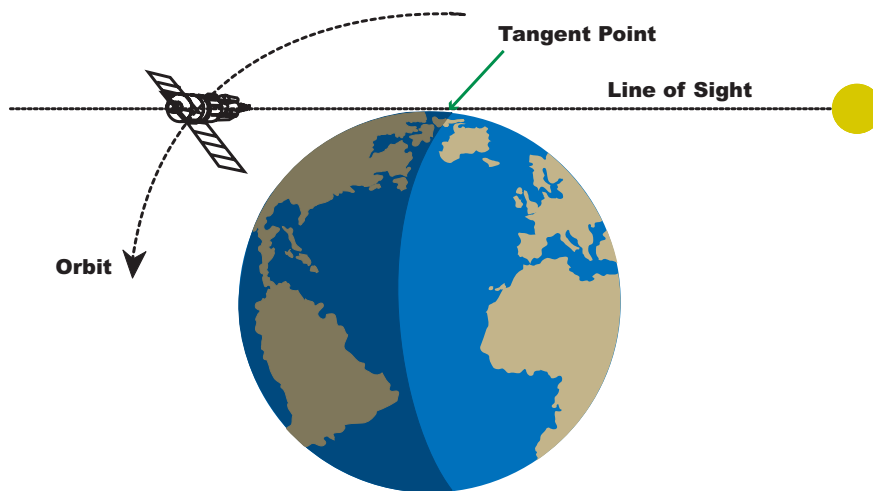


**Figure 3.1: An illustration of solar occultation geometry**

limits solar occultation to about 28-30 events per day. The latitudinal coverage of measurements is dependent on the orbital characteristics of the platform and generally varies quite slowly. Events obtained during the course of one day in a given hemisphere are all at nearly the same latitude. Instruments aboard platforms in sun-synchronous orbits, such as SAM II and POAM II and III, are limited to observations at high northern and southern latitudes whereas instruments in mid-inclination orbits such as HALOE and SAGE II carry out measurements over a broad range of latitudes, albeit requiring from 25 to 40 days to sweep out a full range of latitude. Since these instruments measure direct, unattenuated sunlight before or after each series of measurements, they are effectively calibrated at each measurement opportunity. Consequently, solar occultation instruments are not highly sensitive to changes in instrument performance and are, therefore, well-suited to the detection of long-term trends in measured quantities.

SAGE aerosol products are reported at altitudes between 0.5 and 40.0 km although extinction is often too low to measure above 30 km and the presence of clouds often terminate profiles in the mid and upper troposphere. Termination occurs when the line-of-sight transmission is less than approximately 0.002 which corresponds to nadir optical depths around 0.08 depending on wavelength and the vertical distribution. Typically, the cutoff occurs in the troposphere and is due either to clouds or the solid Earth. However, during the first several years following the 1991 eruption of Mt. Pinatubo, SAGE II events terminated as high as 27 km (in the tropics in late 1991). The loss of data in this period is a significant problem for modeling the climate and chemical changes that occurred as a result of the Pinatubo eruption. The method used to fill this data gap, and the results obtained, are presented in Chapter 4.

Figure 3.2 shows that the 1020 nm aerosol extinction profiles frequently extended to 3 km below the tropopause between 1985 and 1989 (the tropopause altitude is provided as a part of the National Center for Environmental Prediction (NCEP) data products). During this relatively quiet period between 80 and 90 % of all profiles extended down to 3 km below the tropopause. This is typical of the entire SAGE data set except for a few years following the Pinatubo eruption.

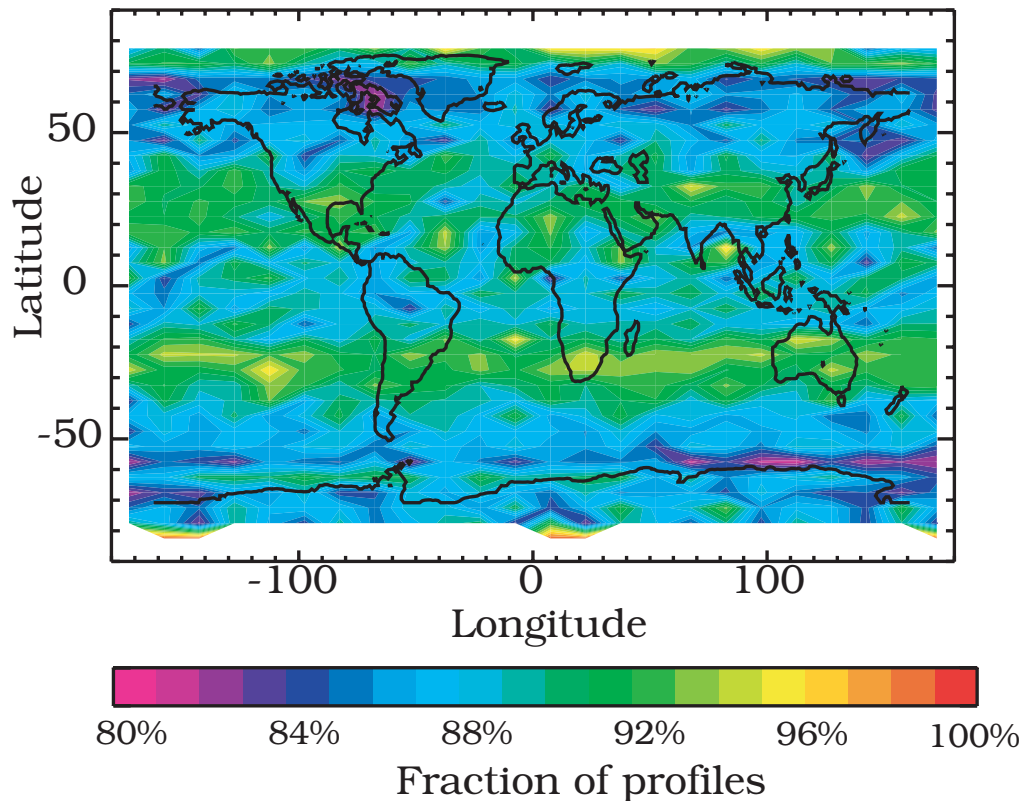


**Figure 3.2:** Mean likelihood of a SAGE II 1020-nm aerosol extinction profile reaching 3 km below the tropopause during the period 1985-1989.

### *SAM II*

The SAM II instrument was a single-channel (1000 nm) sun photometer measuring profiles of aerosol extinction between 10 and 30 km. It flew aboard the Nimbus-7 spacecraft in a sun-synchronous orbit making measurements in both the Arctic and Antarctic. The SAM II data coverage began on 29 October 1978 and extended through 18 December 1993 with a gap between mid-January 1993 and October 1993. From 1978 through 1987 the latitude of the measurement location slowly varied between the lowest latitude (64 degrees at the solstices) and the highest latitude (83 degrees at the equinoxes). However, after 1987, changes in orbit and platform attitude degradation caused the measurement locations to migrate toward the equator.

### *SAGE*

The first SAGE (Stratospheric Aerosol and Gas Experiment) sensor was launched in February 1979 on an Application Explorer Mission satellite and was operational until November 1981. The instrument carried out measurements of solar intensity at four different wavelengths, two of which (450 and 1000 nm) were intended for aerosol extinction determination. SAGE was in a mid-inclination orbit of 56 degrees yielding latitudinal coverage of 80°S to 80°N. During much of its lifetime, a battery problem limited operations to sunset events. The algorithm for the archived version is given in Chu and McCormick [1979].

### *SAGE II*

The SAGE II (Stratospheric Aerosol and Gas Experiment II) sensor was launched into a 57-degree inclination orbit aboard the Earth Radiation Budget Satellite (ERBS) in October 1984 and continues to operate more than 20 years later. This instrument has seven channels nominally at 386, 448, 452, 525, 600, 935, and 1020 nm from which vertical profiles of ozone, nitrogen dioxide, water vapor, and aerosol extinction (at 386, 452, 525, and 1020 nm) are derived. In version 6.1 and later, the base data files also contain aerosol surface area density and effective radius derived using the method described in Thomason et al. [1997b]. Orbital coverage is a function of season and extends from 80°S to 80°N. Following a mechanical fault in July 2000, no data were obtained until December 2000 whereupon operations were resumed at a 50% duty cycle though not restricted by event type. The original algorithm for SAGE II is described in Chu et al. [1989]. Descriptions of the algorithm changes that occurred with the release of 6.0 in June 2000 and 6.1 in October 2001 are described in Thomason et al. [2001].

### *SAGE III*

The SAGE III instrument, launched in December 2001, is a sophisticated descendent of the earlier instruments. The detector is a CCD array (rather than a single wavelength photometer) plus a photodiode at 1545 nm. Aerosol and gas data are obtained at 9 wavelengths (386, 449, 521, 601, 676, 755, 868, 1022, and 1545 nm). We are not using the SAGE III data in this assessment because at the time of writing the data have not been fully validated [Thomason and Taha, 2003].

### *SAGE Processing Procedure*

Measurements by all members of the SAGE series follow the same procedure. When the satellite is about to pass into (or emerge from) the shadow of the Earth, the instrument is activated a few minutes before the platform sunset (sunrise). A detector is used to center the field-of-view (FOV) of the instrument on the azimuthal center of brightness. The instrument then uses a mirror to scan the spectrometer across the Sun vertically relative to the Earth, sampling spectra at 64 Hz (“a packet”). The detection of the edges of the Sun is a key element in locating packets in the atmosphere and on the solar disk. These two elements are, in turn, crucial to the production of all higher-level data products including aerosol extinction as they directly affect altitude registration, measurement noise, and normalization of the data. The scanning process continues throughout the event lasting between 2 and 4 minutes. Events are limited in altitude range to paths that pass within 300 km of the Earth’s surface and by the solid Earth, clouds, or dense aerosol at lower altitudes.

The process of going from measurement to data product is essentially the same for all the instruments in the SAGE series. In fact, future data releases planned for SAGE and SAM II make almost exclusive use of SAGE II processing software. During any sunrise or sunset encountered by the instrument, the instrument FOV is scanned in elevation (altitude) by a mirror at a rate of ~15 arc minutes per second and the spectral channels are sampled at 64 Hz. This results in a series of samples, each spatially overlapping its predecessor by 50 %. The total range of motion of the FOV allows the solar disk to be seen from the Earth's limb to heights greater than 250 km. During a sunrise or sunset event, the FOV tracks the center of brightness of the solar disk in azimuth and is scanned vertically across it in a repetitive up and down pattern. The result of this scanning motion is that a particular altitude in the Earth's

atmosphere is sampled several (typically four or more) times using different portions of the solar disk during an event.

The initial task of the processing is to determine where a particular channel sample was taken in the Earth's atmosphere and what point on the sun was in view. Knowing where each point was taken and which part of the solar limb darkening curve to use in calculating transmission is all that is required to build a line-of-sight transmission profile. To determine the location of each measurement point in the atmosphere and the location of the source point on the solar disk requires knowing the time a scan crosses the edge of the Sun, the location of the spacecraft and the scan rate, as well as accounting for atmospheric refraction. The merit of these quantities directly impacts the accuracy of altitude registration and solar irradiance outside the atmosphere and, ultimately, the quality of the data products. The effect of refraction is a function of altitude, the shape of the Earth, and the density profile of the atmosphere. The spacecraft location is monitored as a part of routine spacecraft operations. The density profile is derived from NCEP reanalysis profiles and the Global Reference Atmospheric Model (GRAM 95) above 55 km.

Once transmission profiles are produced for each instrument channel, profiles of gas species are derived along the line-of-sight using an instrument specific algorithm. For SAM II, which has a single aerosol channel, the algorithm simply subtracts the effects of molecular scatter to produce an aerosol extinction profile. The SAGE I analysis uses a four channel algorithm [Chu and McCormick, 1979] that derives aerosol at 450 and 1000 nm, ozone, and NO<sub>2</sub>. The current SAGE II algorithm [Thomason et al. 2000] uses a revision of the SAGE II version 5.96 species separation processing algorithm that was developed for the Stratospheric Processes and their Role in Climate (SPARC) and United Nations Environmental Programme (UNEP) ozone assessments [SPARC, 1998] and is similar to earlier versions that followed the method described in Chu et al. [1989].

### 3.2.2 HALOE

The Halogen Occultation Experiment (HALOE) is on board the Upper Atmosphere Research Satellite (UARS) and has operated without flaw since its activation on 11 October 1991. The UARS mission is to investigate the global photochemistry, energy balance, and dynamics of the Earth's upper atmosphere. HALOE uses the principle of solar occultation to measure profiles of solar attenuation through the atmosphere's limb, as the sun rises or sets relative to the spacecraft. Measurements in eight infrared bands are used to retrieve the profiles of seven gas mixing ratios (HF, HCl, CH<sub>4</sub>, NO, NO<sub>2</sub>, H<sub>2</sub>O, and O<sub>3</sub>) temperature, and aerosol extinction  $\beta(\lambda)$  at four wavelengths ( $\lambda = 2.45, 3.40, 3.46,$  and  $5.26 \mu\text{m}$ ) [Russell et al., 1993]. HALOE measurements cover two longitude sweeps each day (15 profiles each), one at the latitude of sunsets and one at the latitude of sunrises. The progression of measurement latitude with time provides near global coverage over periods of 3-4 weeks, as demonstrated in Figure 3.3. The instrument field of view projected at the limb is 1.6 km vertically by 6 km horizontally. Optical effects and electronic smoothing yield an effective vertical resolution of  $\sim 2$  km, corresponding to a tangent point path length of  $\sim 320$  km.

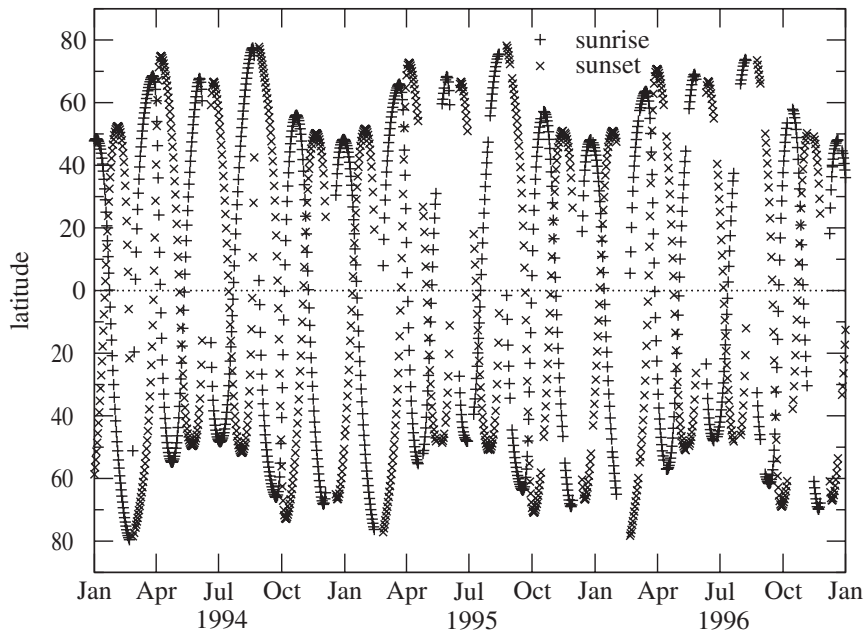


**Figure 3.3: HALOE latitude coverage versus time for the period from 1994 to 1996. Symbols represent daily average latitude for either sunrise or sunset measurements.**

HALOE aerosol extinction retrievals are accomplished using measurements from four gas correlation channels [Hervig et al., 1995]. For these measurements, the incoming radiation for each channel is split into two paths. One path passes through a cell containing a sample of the gas to be measured (e.g., HCl) and the other passes through vacuum. The difference of these two signals is insensitive to aerosols, and allows accurate retrieval of the target gas abundance. Once the target gas mixing ratio profile is retrieved, it is then used to subtract the gaseous signal from the vacuum path measurement. The remaining vacuum path signal is due only to aerosols, and is then used to retrieve profiles of aerosol extinction. Aerosol extinctions are retrieved at the over-sampled vertical spacing of 0.3 km, and have uncertainties on the order of  $\pm 10\text{-}15\%$  [Hervig et al., 1996]. Because gaseous interference must be removed to retrieve aerosol extinction, errors in HALOE aerosol extinctions are lowest when the aerosol signal is large compared to the gaseous contribution. Within the HALOE time-frame, the lowest extinction uncertainties are associated with the early 1990s when Pinatubo aerosols were present. Extinction uncertainties increase with dissipation of the Pinatubo aerosols. HALOE aerosol retrievals extend in altitude from the upper troposphere to about 90 km. Above the stratospheric aerosol layer (roughly 35 km), aerosol retrievals serve primarily to characterize polar mesospheric clouds. The lower limit for measurable extinction is determined by the signal digitization where one bit corresponds to an aerosol extinction of  $2 \times 10^{-6} \text{ km}^{-1}$ . Measurement noise inherent to the electro/optical system raises the extinction noise floor to about  $5 \times 10^{-6} \text{ km}^{-1}$ . The limb view becomes completely opaque for aerosol extinctions greater than about  $10^{-2} \text{ km}^{-1}$ .

HALOE measurements have been used to characterize a variety of atmospheric particles including stratospheric sulfate aerosols, cirrus clouds, polar stratospheric clouds (PSCs), and polar mesospheric clouds (PMCs). Since this assessment is concerned with stratospheric aerosols, clearing measurements of other particle types within HALOE data is necessary. Tropospheric cloud tops were identified in HALOE profiles using two indicators described

by Hervig and McHugh [1999]. In one approach, the rapid increase in extinction associated with cloud tops was found to be a reliable cloud top indicator. In a second approach, uniformity among the four HALOE extinctions provides another reliable cloud indicator, because the large particles associated with cirrus produce relatively flat extinction spectra when compared to aerosol extinction. These two cloud identifiers were not confused by the presence of volcanic aerosols. Stratospheric cloud identification was accomplished using the vertical extinction gradient for results presented in this report. An example of the cloud top frequency distribution determined from HALOE measurements during 1998 is shown in Figure 3.4. A record of cloud tops identified in HALOE profiles is available on the HALOE web site: <http://haloedata.larc.nasa.gov/Haloe/home.html>.

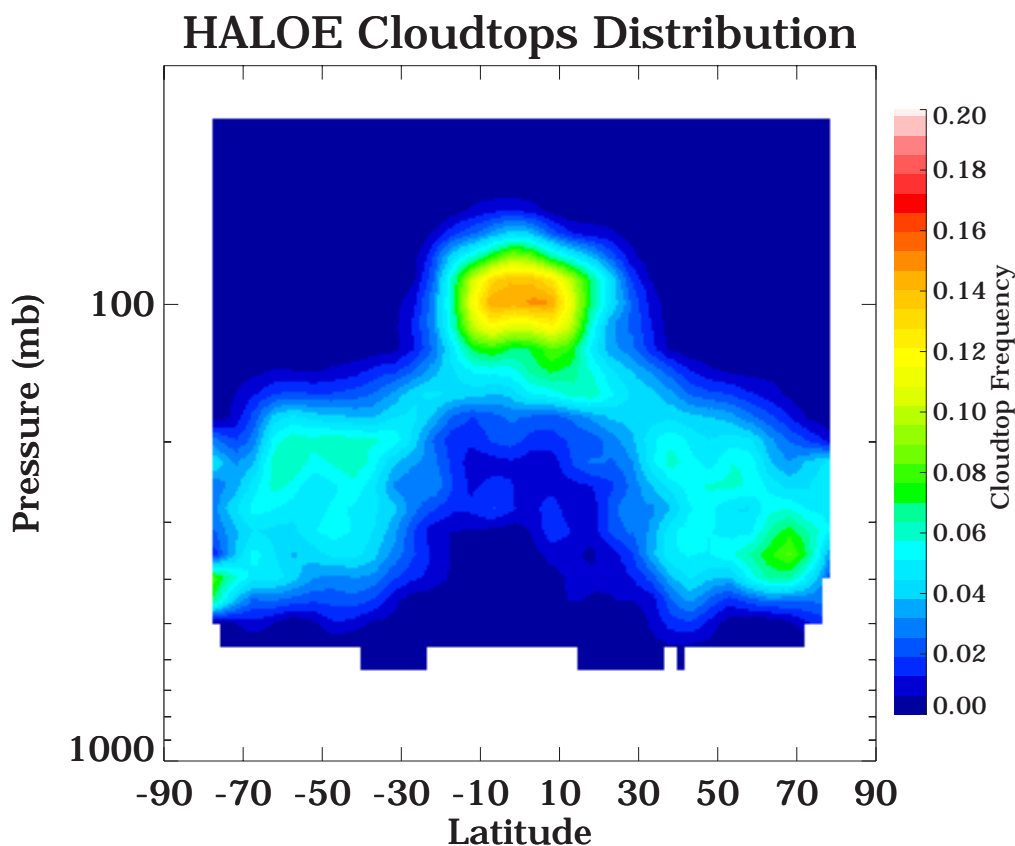


**Figure 3.4:** The cloud top frequency distribution determined from HALOE measurements during 1998.

### 3.2.3 POAM II and POAM III

The Naval Research Laboratory's Polar Ozone and Aerosol Measurement II (POAM II) was a satellite-based visible/near infrared photometer for making measurements of constituents in the polar stratosphere. POAM II measured atmospheric slant optical depth in nine narrow band channels from 0.352 to 1.060  $\mu\text{m}$ . These measurements were used to retrieve ozone, water vapor, nitrogen dioxide, and aerosol extinction at five wavelengths (0.353, 0.442, 0.780, 0.920, and 1.060  $\mu\text{m}$ ). POAM II was launched aboard the French SPOT-3 satellite in September 1993 into a Sun synchronous polar orbit, and made measurements until the host satellite failed in November 1996. As seen from the satellite, the Sun rose in the Northern

Hemisphere and set in the Southern Hemisphere roughly 14 times per day, providing 14 measurements daily in each hemisphere around a circle of latitude. Sunrise measurements were made in a latitude band from 54-71°N, while sunsets occurred between 63-88°S. The POAM II instrument and mission is described in detail by Glaccum et al. [1996]. The POAM II measurements have been applied to studies of ozone, aerosols and PSCs in the Antarctic and the Arctic (see, e.g., Bevilacqua [1997] and references therein).

The POAM II version 5 retrieval algorithm is described and characterized (including a detailed error analysis) by Lumpe et al. [1997]. For the purposes of this report, the most important aspect of the POAM II retrieval algorithm is that, in the separation of the total measured optical depth into its specific components, the aerosol component is not determined separately in each spectral channel. Rather, the wavelength dependence of the aerosol slant optical depth,  $\delta_{i(\text{aerosol})}$ , at each tangent altitude is constrained by the following parameterization:

$$\ln(\delta_{i(\text{aerosol})}) = \mu_0 + \mu_1 \kappa_i + \mu_2 \kappa_i^2 ,$$

where the  $\mu_j$  are the effective aerosol coefficients retrieved in the algorithm, and  $\kappa_i \equiv \ln(\lambda_i)$ , with  $\lambda_i$  being the central wavelength of channel  $i$ . This functional form provides a smooth spectral dependence of aerosol optical depth that has been found to fit a large range of stratospheric aerosol models [Lumpe et al., 1997].

The final, archived POAM II retrieval version is version 6. The main differences between the version 5 and 6 algorithms can be summarized as follows: (1) the version 6 retrievals use temperature/pressure profiles obtained from the United Kingdom Met Office (UKMO) analysis instead of the NCEP analysis used in version 5 for the specification and removal of Rayleigh scattering from the measured slant optical depths, and (2) in version 6,  $\text{NO}_2$  is retrieved simultaneously with ozone and aerosol extinction whereas in version 5,  $\text{NO}_2$  was fixed at climatological values. The aerosol parameterization and retrieval methodology employed in the version 6 algorithm are identical to that used in version 5 described briefly above and in detail by Lumpe et al. [1997].

The vertical resolution of the POAM II aerosol extinction retrieval, defined as the full-width-half-maximum of the retrieval averaging kernels, is about 1.2 km at 20 km with resolution values increasing at lower altitudes to about 2 km at 10 km, and at higher altitudes to about 2.5 km at 25 km. The precision of the 1.060  $\mu\text{m}$  aerosol extinction retrieval is estimated to be about 10 %, roughly independent of altitude below 25 km. At 0.442  $\mu\text{m}$  the random error is about 12 % at 18 km, increasing with both increasing and decreasing altitude to near 30 % at 12 km and 20 % at 25 km [Randall et al., 2000]. The POAM II aerosol extinction measurements have been validated by comparison with balloon-borne polarimeter and lidar measurements by Brogniez et al. [1996], and with SAGE II measurements by Randall et al. [1996, 2000]. POAM II measurements of the seasonal variation of stratospheric aerosol extinction at polar latitudes, and the decrease of volcanic aerosol over the period November 1993 through February 1996, from the Mt. Pinatubo eruption, are presented by Randall et al. [1996].

The POAM II mission was terminated by a satellite failure in November of 1996. A follow-on instrument, POAM III, was subsequently launched in March 1998 aboard SPOT-4, and is still operational at the time of this writing. The orbit is identical to that of POAM II, providing a direct extension of the POAM II data record in time. The POAM III instrument is similar to POAM II, but includes several design improvements. Many of the measurement channels (especially the 0.354  $\mu\text{m}$  channel) have much higher signal-to-noise ratios than that ob-

tained in POAM II. The sun sensor is also more sensitive, enabling POAM III to routinely measure lower into the atmosphere. Also, the wavelengths and bandwidths of the science channels differ slightly from those in POAM II. The POAM III aerosol channels are 0.354, 0.442, 0.779, 0.922, and 1.020  $\mu\text{m}$ . In this regard, the only significant difference is that the red channel has been moved from 1.060 in POAM II to 1.020  $\mu\text{m}$  (i.e., identical to SAGE II) for POAM III. The POAM III interference filters were manufactured using an ion assisted deposition process. Both the center wavelength and bandpass of these filters have been shown to be very stable in extensive testing under extreme environmental conditions [Heath et al., 1997, 1998]. The POAM III instrument is described in detail by Lucke et al. [1999].

In August 2004, the operational POAM III retrieval algorithm was upgraded from version 3 to version 4, and the entire data set was reprocessed. The version 3 retrieval algorithm is described and characterized in detail by Lumpe et al. [2002]. (It might be noted that version 3 for POAM III is similar to version 6 for POAM II.) The most significant changes between the version 3 and 4 algorithms are:

1. As in version 3, altitude registration at higher altitudes is determined by maintaining the expected slant optical depth ratios between channels that are dominated by Rayleigh scattering, and at lower altitudes by using the instrument potentiometer (which gives the instrument pointing angle with respect to the spacecraft). As explained by Lumpe et al. [2002], in version 3 the transition between these two approaches for determining the pointing occurred at about 34 km, whereas in version 4 it has been pushed down to about 26 km.
2. The calibration of the instrument potentiometer, used for altitude registration below 26 km, has been improved in version 4, and is less susceptible to errors resulting from small variations in the non-linearity of the potentiometer.
3. The parameterization of the spectral dependence of the aerosol slant optical depth (optical depth versus wavelength) used in the aerosol extinction retrieval has been changed from the quadratic in the log of the slant optical, used in the version 3 retrievals (and the POAM II retrieval algorithm), to a quadratic in the optical depth directly. This simple, linear parameterization leads to a faster and more robust gas species retrieval without loss of accuracy in the aerosol extinction retrieval.

Estimated random errors in the POAM III aerosol extinction profiles at 1.02  $\mu\text{m}$  are 10-15 % below 23 km, increasing to 30 % at 25 km. At 0.442  $\mu\text{m}$  they range from 10 % above 15 km, increasing to about 20 % at 12 km. These estimates are roughly similar to the POAM II values at 1.02  $\mu\text{m}$ , but are somewhat smaller than the POAM II values at 0.442  $\mu\text{m}$ . The vertical resolution of the POAM III aerosol extinction retrievals is 1-1.5 km (that is, somewhat higher than the POAM II aerosol extinction retrieval both near the tropopause and at 25 km) for all aerosol channels up to 25 km. The POAM III (version 3) aerosol extinction measurements have been validated by Randall et al. [2001] through extensive comparisons with both SAGE II and HALOE.

### 3.3 Global Short-Term Measurements

#### 3.3.1 CLAES

##### *The CLAES Instrument and the Measurement Process*

The Cryogenic Limb Array Etalon Spectrometer (CLAES) was one of ten complementary experiments launched on the Upper Atmosphere Research Satellite (UARS) in 1991. CLAES measured concentrations of ozone, methane, water vapor, nitrogen oxides, CFCs, temperature, and aerosol absorption at multiple wavelengths. These measurements were analyzed to develop a better understanding of the photochemical, radiative, and dynamical processes taking place in the ozone layer.

CLAES analysis inferred concentrations of stratospheric constituents from the measurement of infrared emission features associated with each gas. To separate the often very weak signatures of trace gases such as CFCs from the background radiation requires both high spectral resolution and high sensitivity. This was done by combining a telescope with an infrared spectrometer and solid state detectors, and cryogenically cooling the whole instrument to prevent its own thermal infrared emissions from interfering with the measurement of weak atmospheric signals. The spectrometer had a resolving power of about 4000 and operated over the wavelength range 3.5 to 12.9  $\mu\text{m}$ .

The instrument consisted of a front-end sensor, made up of the telescope, spectrometer, and detectors, and the back-end cryogenic cooler, made up of an inner tank of solid neon (at  $-257^{\circ}\text{C}$ ) and a surrounding tank of solid carbon dioxide (at  $-150^{\circ}\text{C}$ ). The entire instrument was kept under vacuum during ground test and launch, and then exposed to the vacuum of space when the telescope door was opened in orbit. The cryogenics, which slowly evaporated as they cooled the instrument, were designed to last about 19 months in orbit. CLAES made scientific measurements from 1 October 1991 through 5 May 1993, when the cryogenics had fully evaporated and the instrument warmed up. CLAES was approximately 2.7 m long and 1.2 m in diameter, used an average of about 25 watts of power in orbit, and had a mass of about 1200 kg when loaded with cryogen.

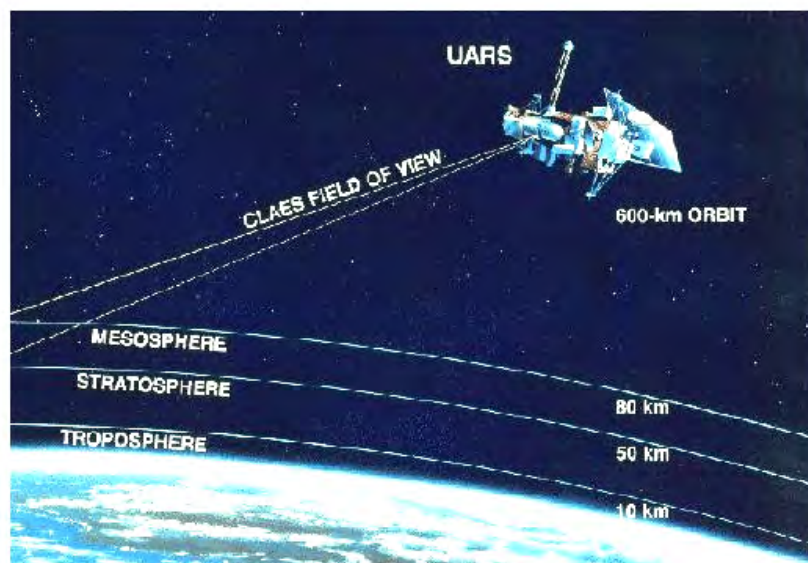


Figure 3.5: CLAES limb viewing geometry

CLAES looked out from one side of the UARS spacecraft at a fixed  $90^\circ$  angle to the velocity vector and was mostly pointed above the earth horizon (or “limb”) to observe the upper atmosphere between about 10 and 60 km above the surface, as shown Figure 3.5. This is the region encompassing the stratosphere and the lower mesosphere.

The instrument used an array of detectors providing 20 “footprints” at the earth limb between the 10 and 60 km altitude levels, each one separated by 2.5 km to provide vertical profiles of each gas with this vertical resolution. The UARS orbit had a  $57^\circ$  inclination and this allowed CLAES to view to  $80^\circ$  latitude in one hemisphere, and to  $34^\circ$  in the other. This orbit precessed  $180^\circ$  in about 36 days relative to the Sun. Because of this, UARS was rotated  $180^\circ$  in yaw approximately every 36 days such that one side of the spacecraft was kept facing away from the sun and instruments on this side, including CLAES, would stay cool. This meant that CLAES alternately viewed from  $34^\circ\text{N}$  to  $80^\circ\text{S}$  or  $34^\circ\text{S}$  to  $80^\circ\text{N}$  in 36 day periods. For a more detailed instrument description see Roche et al. [1993].

Figure 3.6 shows the latitude/longitude tracks of the center of the CLAES field of view at the earth limb for one day for a north-looking case. A south-looking case would look essentially the same, with the latitude limits changed to  $34^\circ\text{N}$  and  $80^\circ\text{S}$ . There are 15 orbits per day, and since CLAES took about 65 seconds for a complete measurement cycle it acquired about 1300 measurement sets per day. As the figure shows, measurement tracks are particularly dense near the polar regions, allowing for good coverage of ozone-related chemistry and dynamics over the Arctic and Antarctic.

CLAES produced a 19-month global database of stratospheric gases and aerosol and their variation with time of day, season, latitude, and longitude.

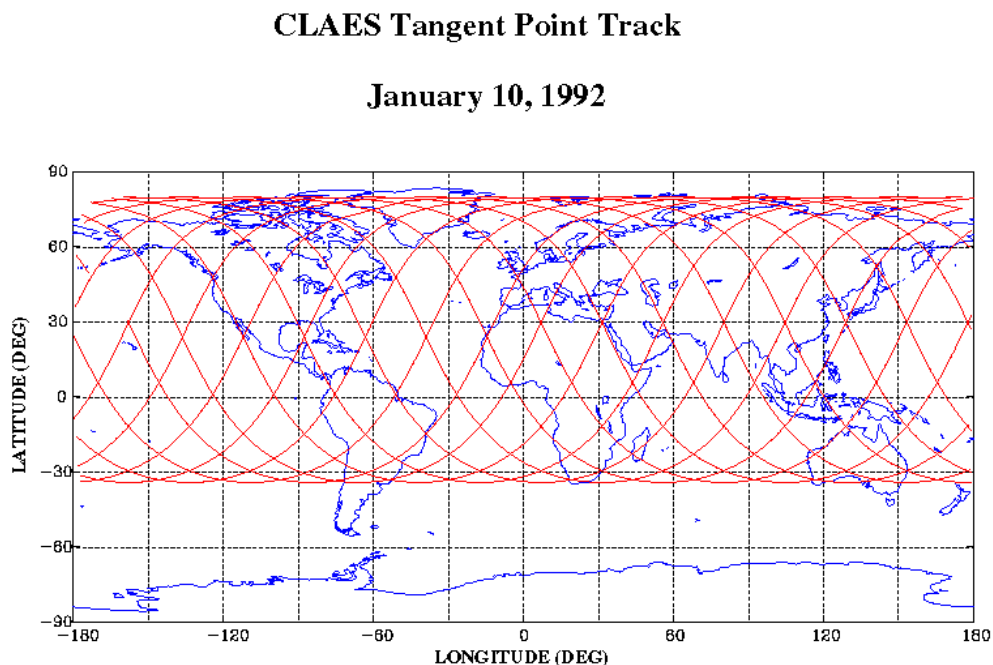


**Figure 3.6: CLAES sampling for a “northern look” ( $34^\circ\text{S}$  to  $78^\circ\text{N}$ ). Coverage alternated between this and the “southern look” ( $34^\circ\text{N}$  to  $78^\circ\text{S}$ ) about every 36 days.**

*CLAES aerosol measurements and data*

CLAES acquired medium resolution spectra of infrared thermal emission from the Earth's limb in nine channels ranging from 3.5 to 12.8  $\mu\text{m}$  and over an altitude range of approximately 10-60 km. Vertical profiles of temperature, several gaseous species (NO, NO<sub>2</sub>, H<sub>2</sub>O, CH<sub>4</sub>, N<sub>2</sub>O, N<sub>2</sub>O<sub>5</sub>, CFC-11, CFC-12, HNO<sub>2</sub>, ClONO<sub>2</sub> and O<sub>2</sub>) and aerosol volume absorption coefficient for each channel (7 channels, 5.3 to 12.8  $\mu\text{m}$ ) were inferred from the limb radiance measurements. During the CLAES lifetime, stratospheric aerosol levels were quite elevated due to the 15 June 1991 eruption of the Mt. Pinatubo volcano in the Philippines. Because the infrared channels did not saturate, and thermal emissions provide relatively high density coverage, the CLAES data set is the most comprehensive limb view of the decay of the Pinatubo aerosol. The spectral micro-windows were chosen to contain emission features of a target gas, but they also contain information in the continuum emission which can be used to estimate aerosol loading. This requires knowledge of pressure and temperature; these were determined from a multi-emitter multi-channel onion-peeling retrieval applied to the micro-window targeting the 790.2  $\text{cm}^{-1}$  CO<sub>2</sub> Q-branch. Given this temperature/pressure knowledge, the continuum emission in each of the other channels was processed to yield aerosol volume absorption coefficients in the remaining micro-windows. The retrieval process is based on the development of Rodgers [1976] and is described by Kumer et al. [1996]. There were three releases of the CLAES processing software (versions 7, 8, and 9) with incremental improvements in each data set. The aerosol validation paper, Massie et al. [1996], was written using V7 data. Differences between V7 and later versions including the current V9 data are available on the Goddard Distributed Active Archive Center (DAAC).

CLAES products include "Level 1" or calibrated limb radiance data, "Level 2" retrieved products on their native 2.5 km vertical grid, and "Level 3 Along Track" (L3AT) aerosol volume absorption coefficients. These retrieval products are interpolated in time along the tangent point observation path to the center of the 65.3 second sampling interval, and in pressure to the standard UARS surfaces defined by  $p = 10^{3-N/6}$  hPa where  $N$  is the layer index. Aerosol data are recorded for levels from 346 hPa to about 0.1 hPa. The primary validation paper for these data [Massie et al., 1996] focuses on the region from 100 hPa to about 10 hPa. The layers centered at 215, 146, 100 and 68 hPa ( $N = 4, 5, 6$  &  $7$ ) cover the region where tropical cirrus clouds are likely to be seen in CLAES data. Cirrus and PSCs are included in the aerosol data and must be separated from the sulfate aerosol with some process such as the threshold method developed in Mergenthaler et al. [1999].

### 3.3.2 ORA

The Occultation Radiometer (ORA) instrument on the European Retrievable Carrier (EURECA) satellite was launched in August 1992 and placed in a low inclination orbit. The instrument was equipped with eight broadband channels in the 0.259-1.013  $\mu\text{m}$  range [Arijs et al., 1995]. It measured ozone [Fussen et al., 2000], nitrogen dioxide, water vapor and aerosol extinction profiles from August 1992 up to May 1993 in the 40°S-40°N latitude range and therefore provided a unique opportunity to observe the Mt. Pinatubo aerosol [Fussen et al., 2001b, 2001c]. About 7000 orbital sunsets and sunrises were measured during this period.

Although the apparent vertical resolution is poor (about 25 km, defined to be the solar size at the tangent point) due to the simplicity of the optical design, the very large signal-to-noise ratio allowed a final vertical resolution of 2-3 km to be obtained. Also, aerosol extinction profiles could be retrieved for altitudes lower than possible with more sophisticated

instruments such as SAGE II. This required, however, the use of complex inversion algorithms [Fussen et al., 1997, 2001a]. The comparison of data with other experiments showed fairly good agreement for aerosol extinction [Fussen et al., 1998] and optical thickness [Vanhellemont et al., 2000] and for derived aerosol parameters [Bingen et al., 2002].

### 3.4 Localized Long-Term Measurements

#### 3.4.1 Balloon Borne Optical Particle Counter

Stratospheric aerosol measurements at Laramie, Wyoming, began in 1971 using an optical particle counter (OPC) initially developed by Rosen [1964]. The instrument, a white light counter measuring aerosol scattering at 25° from the forward direction, is a single particle counter. Mie theory is used to determine aerosol size [Mie, 1908]. An incandescent lamp, optics, and light controller supply a stable image of the incandescent lamp filament in the scattering region that is larger than the aerosol sample stream, thus edge effects are not a problem in defining sample volume. Light scattered from single particles passing through the beam is collected over a solid angle of ~ 0.17 steradian and focused onto a photomultiplier tube (PMT) for pulse height detection. Two symmetrical independent photon paths use coincidence to limit noise, Rayleigh scatter, and the influence of cosmic rays. Single coincident PMT pulses exceeding preset voltage levels are counted, determining size and number concentration. Prior to each flight the instruments are calibrated with polystyrene latex (PSL) spheres and the pump flow rate measured. Periodically the stability of the pumps throughout flight range pressures is checked, and the theoretical counter response function checked against PSL and monodispersed diethyl hexal sebacate at several sizes. See Deshler et al. [2003] for additional details.

Initial measurements in the 1970s consisted of measurements of particles  $r > 0.15$  and  $> 0.25 \mu\text{m}$  at a sample flow rate of  $1 \text{ liter min}^{-1}$  [Pinnick and Hofmann, 1973; Hofmann et al., 1975]. In 1989 the OPC was modified to make measurements for particles  $> 0.4 \mu\text{m}$ , to increase the number of sizes measured, and to decrease the minimum concentration measurable. This was done to use the instrument to measure PSC particles  $> 0.4 \mu\text{m}$  because of the importance of these particles in polar ozone loss [Solomon et al., 1986]. The scattering angle of the detector axis was increased from 25 to 40° and the air sample flow rate increased from 1 to  $10 \text{ liter min}^{-1}$ , with appropriate changes in inlet design to maintain roughly isokinetic sampling. This new scattering angle allowed unambiguous detection of particles throughout the size range 0.15-10.0  $\mu\text{m}$  in twelve size bins. Minimum detectable concentrations for this improved OPC are  $6 \times 10^{-4} \text{ cm}^{-3}$  as opposed to  $6 \times 10^{-3} \text{ cm}^{-3}$  for the initial OPC. The improved OPCs were first used in Antarctica in September 1989 [Hofmann and Deshler, 1991]. After calibration flights in Laramie to insure that the measurements at 0.15 and 0.25  $\mu\text{m}$  radius are the same, within measurement limits, for the OPC with scattering angle at 25 and at 40°, the 40° OPC has replaced the original OPC also for the flights from Laramie [Deshler et al., 1993; Deshler et al., 2003]. Measurements with the 40° OPC from Laramie began in 1991. Tests with both OPCs continued until 1994 comprising 22 comparison flights. Current measurement capabilities consist of condensation nuclei (CN,  $r > 0.01 \mu\text{m}$ ) and optically detectable aerosol,  $r \geq 0.15$ -2.0 or 10.0  $\mu\text{m}$  in twelve size ranges, from the surface to 30 km. The strength of these in situ measurements is in providing measurements easily converted into size distributions, from which other quantities of interest, e. g. aerosol surface area, or extinction, can be calculated. Additional details concerning the instrument function and laboratory tests are provided by Deshler et al. [2003].

Before each flight an OPC is calibrated by adjusting instrument gain until measured instrument response is consistent with theoretical instrument response for measurements on well characterized monodisperse aerosol. Instruments are calibrated using commercially available PSL spheres near  $0.5 \mu\text{m}$  radius, a standard aerosol which has been used since the 1970s. It is sufficient to calibrate the instrument using only one particle size; however, the theoretical counter response curve has been checked a number of times using monodisperse particles of several sizes and different refractive indices [Pinnick and Hofmann, 1973; Zhao, 1996; Miao, 2001; Deshler et al., 2003].

Aerosol sizing errors result primarily from pulse width broadening of the PMT response for a constant optical input. Variations in intensity of the light beam, and variations in aerosol paths through the beam play secondary roles. These errors lead to sizing errors which are a function of index of refraction since the shape of the counter response curve varies with index of refraction. For temperatures above  $-65^\circ\text{C}$  and water vapor concentrations near 5 ppmv, the real part of refractive index for sulfuric acid aerosol varies from 1.43 to 1.45, with no absorption [Steele and Hamill, 1981; Russell and Hamill, 1984]. Variations of index of refraction in this range lead to sizing errors well below those associated with the pulse width broadening discussed above, and do not contribute significantly. Counter response curves from Pinnick and Hofmann [1973] and Deshler et al. [2003], and the measured pulse width broadening from the phototubes leads to a sizing error of  $\pm 10\%$  at  $0.15$  and  $0.25 \mu\text{m}$  for a nominal index of refraction of 1.45.

Errors in concentrations measured by these instruments depend on variations in air sample flow rate, the reproducibility of a measurement from two identical instruments, and Poisson counting statistics. The pumps used for these instruments are constant volume gear displacement pumps. In laboratory tests pump flow rates are found to decrease by 3 % at ambient pressures of 30 hPa and by 13 % at 5 hPa [Miao, 2001]. These variations are, however, less than other uncertainties, and concentration measurements are not corrected for measurements at low pressures. Laboratory tests with two identical counters on several samples of differently sized monodisperse aerosol indicate a measurement precision of  $\pm 10\%$  for relatively high concentrations of aerosol when Poisson counting statistics are not a factor.

Poisson counting statistics define the fractional uncertainty of a count as its inverse square root,  $C^{-0.5}$  for  $C$  counts in one sample, becoming important at low concentrations. The aerosol concentration,  $N = C \times S / F$  for sample frequency  $S$  and flow rate  $F$ . Thus the Poisson error fraction, in terms of concentration, is  $(N \times F / S)^{-0.5}$ . For these instruments:  $S = 0.1$  Hz,  $F = 16.7 \text{ cm}^3 \text{ s}^{-1}$  for the  $25^\circ$  OPC, and  $F = 167 \text{ cm}^3 \text{ s}^{-1}$  for the  $40^\circ$  OPC. In the stratosphere these ambient air flow rates are reduced to about 80 % of these values by temperature differences between outside air and pump. This leads to uncertainties of 85, 25, and 8 % for concentrations of 0.01, 0.1,  $1.0 \text{ cm}^{-3}$  at the low flow rate and concentrations of 0.001, 0.01,  $0.1 \text{ cm}^{-3}$  at the high flow rate. Poisson counting errors dominate at concentrations below 0.1 ( $0.01$ )  $\text{cm}^{-3}$  for the low (high) flow rate instrument. At concentrations higher than these a concentration error of  $\pm 10\%$  reflects measurement precision.

### 3.4.2 Lidar Systems

Lidars are active remote sensing instruments analogous to radar, but using optical wavelengths. (“Lidar” is the acronym for “LIght Detection And Ranging.”) Lidars came about with the development of very short single pulses of laser energy, capable of illuminating a narrow atmospheric column. The return signal is collected and the time between the emitted laser pulse and the scattered return signal is proportional to the altitude at which the scattering occurred. Properties accessible to a lidar are linked to the interaction between radiation and matter, which in turn depends on the nature of the particles and on the type of scattering/absorption being studied [Measures, 1984]. Specifically, with a lidar, one can measure Rayleigh scattering, Mie scattering, Raman scattering, resonance scattering, fluorescence, and absorption. Multi-wavelength lidars can measure differential absorption and scattering. The earliest lidar experimental applications were devoted to atmospheric dust and aerosol layer observations [Fiocco and Smullin, 1963; Fiocco and Grams, 1964; McCormick et al., 1966].

Spectral properties of the elastic scattering of light by particles of radii ranging from about 0.05 to 100  $\mu\text{m}$  are described by Mie theory, under the assumption of particle sphericity and homogeneity. The optical properties of particles measured by lidar are determined by their composition (refractive index), by their phase (liquid/solid) and by their size distribution. In principle, these parameters can be retrieved through lidar signal inversion, but in reality, there are too many unknowns for a single equation. Indeed, in the basic lidar equation, optical properties at each range are determined by the elastic backscatter at that range and attenuation along the two-way path, which contains both a molecular contribution (Rayleigh scattering) and a particulate contribution (Mie scattering). The molecular atmosphere is accounted for by using correlative atmospheric density profiles from either radiosonde profiles, atmospheric models or temperature Raman lidar profiles [Keckhut et al., 1990]. A critical assumption is the relationship between the backscatter cross-section and the extinction cross-section. Klett [1981] showed that such relationships are highly variable as they require an *a priori* knowledge of particle shape and chemical composition.

Particular lidar applications allow one to derive aerosol extinction coefficients independent of the aerosol backscatter. In the High Spectral Resolution Lidar (HSRL) approach, the aerosol and molecular scattering contributions are separated on the basis of the much wider Doppler broadening of molecular scattering [Shipley et al., 1983]. Vertical profiles of aerosol extinction and backscatter coefficients can be independently determined simultaneously using elastic (Rayleigh-Mie) and inelastic (Raman) backscatter lidar signals [Ferrare et al., 1998].

Considerably more information is available in the received wave by considering its polarization characteristics. Indeed, for single scattering, Rayleigh backscatter from atmospheric gases and Mie backscatter from spherically symmetric particles retain the incident polarization to within 2%. Consequently, the most likely sources of any observed depolarization would be the irregular shape and multiple scattering.

Most lidar measurements of stratospheric aerosols are made using single wavelength systems. The choice of the wavelength is not critical for an aerosol lidar, but there are two points considered by researchers in selecting the operating wavelength: first, to avoid atmospheric gaseous spectral absorption regions (i.e.,  $\lambda \leq 1000$  nm approximately), and second, to pick a wavelength long enough so that the aerosol scattering signal is not too small compared to the molecular Rayleigh scattering (i.e.  $\lambda \geq 300$  nm). Typically, the range goes from near UV to near IR. Most aerosol lidars use the 532 nm wavelength, which is the second harmonic of

Nd:YAG lasers. The fundamental (1064 nm) and third (355 nm) harmonics are also used. Traditionally, the relative particulate contribution to backscatter is represented at each range by the backscatter ratio, defined as the ratio of the total to molecular backscatter coefficient. A backscatter ratio greater than 1 indicates the presence of scatterers distinct from the molecular atmosphere.

The strength of an aerosol lidar is its ability to yield information on the morphology and structure of the aerosol layers, with very high vertical and temporal resolutions, and the prospect of obtaining long-term series. The direct products are optical properties so aerosol lidars are not instruments of "remote spectroscopy" and the retrieval of the physical properties of the particles requires a priori knowledge and assumptions. Meanwhile, indirect retrieval of particle properties is made possible by the combination of lidar observations together with in situ instruments (optical counters, for instance), other optical sensors (giving a multispectral approach) or using model constraints.

#### *Integrated Backscatter from Various Lidar Systems*

Less than one decade after the first lidar atmospheric applications were developed, the applicability of this technique to long-term monitoring of stratospheric aerosols became apparent [Fiocco and Grams, 1964]. The first operational routine measurements were carried out in the early 70's with instruments using a sodium laser at 589 nm (as in Saõ José Dos Campos, Brazil) or a ruby laser at 694 nm (as in Hampton, USA, Garmisch-Partenkirchen, Germany and Mauna Loa, USA). Since the end of the 1980s, most of the instruments have used Nd:YAG lasers at 1064 nm, frequency doubled to emit at 532 nm or frequency tripled at 355 nm.

Today, lidar systems are operated routinely all over the world, at all latitude bands, but with the majority located in the Northern Hemisphere. Table 3.2 gives a list of the various stratospheric aerosol lidars operated in the past or still running today, from Arctic to Antarctic latitudes. The geographical locations, the time frames and the operating wavelength are given, together with the updated names of investigators.

Some lidar stations, often included in national or international long-term stratospheric monitoring programs, provide quasi-continuous long-term records, with a high operation rate. In general, operations are only interrupted for technical reasons or during the summer periods (daytime) in the polar regions. These lidar stations can provide suitable datasets for establishing a stratospheric aerosol climatology. Their location is shown on Figure 3.7 and their characteristics and integrated backscatter records are given below.

#### *Ny-Alesund – Arctic*

Stratospheric aerosol and PSC observations are performed at Ny-Alesund, Spitsbergen (78.92°N, 11.93° E) using a multi-wavelength and polarization backscatter lidar instrument [Beyerle et al., 1994; Biele et al. 1997; Biele et al., 2001]. The station is the Primary Arctic Station of the Network for the Detection of Stratospheric Change (NDSC).



**Figure 3.7:** Map showing the locations of the lidar stations providing long-term continuous series of stratospheric observations.

Measurements shown in Chapter 4 use the second harmonic of a Nd:YAG laser at a wavelength of 532 nm operating with a pulse repetition frequency at 30 Hz. Laser pulse energy is typically 180 mJ. The backscattered signals are collected by a 60 cm telescope (field of view 0.8 mrad), separated according to wavelength and perpendicular/parallel polarization and detected by sensitive photomultipliers in photocounting mode. A mechanical chopper prevents saturation of the photodetectors by signals from low altitudes. The vertical resolution varies over different years from 15 to 200 m. The instrument was refined and improved several times during the period. The atmospheric density profile is calculated from pressure and temperature profiles measured daily by the local meteorological radiosonde. The lidar signal inversion is based on the Klett [1981, 1985] method.

#### *Garmisch-Partenkirchen – Northern Middle Latitude*

Measurements at Garmisch-Partenkirchen, Germany (47.48°N, 11.06°E) began in 1976 and are focused, among other parameters, on the stratospheric aerosol [Reiter et al., 1979; Jäger, 1991, Jäger, 2005]. The station is part of the northern mid-latitude primary station of NDSC, (Alpine Station).

Early observations were obtained with a ruby lidar system at 694 nm. Between 1990 and 1991, observations were interrupted to rebuild the lidar system. Measurements starting in 1991 use the 532 nm second harmonic of the Nd:YAG laser, emitting, at this wavelength, about 600 mJ at a 10 Hz repetition rate. Lidar signals are received on a 52 cm diameter Cassegrain telescope. Vertical resolution was typically 600 m with the ruby system, and is typically 75 m with the Nd:YAG system. All 532 nm aerosol optical parameters are converted into 694 nm values to easily compare them with earlier measurements obtained with the ruby laser. Molecular density is derived from radiosonde profiles made at Munich, 100 km north of the lidar location.

Backscatter integrations cover the altitude range from the tropopause + 1 km to profile top (around 30 km). Error estimates range from 10 to 50 %, depending on stratospheric aerosol load, for the ruby measurements. These errors are reduced by about half for the 532 nm measurements.

#### *Observatoire de Haute-Provence – Northern Middle Latitude*

The Observatory of Haute-Provence (OHP, 43.94°N, 5.71°E), located in the South-East of France, is one of the four French Atmospheric Observatories (with Dumont d'Urville, Alomar and La Réunion Island). The OHP station is part of the mid-latitude primary station of NDSC in the Northern Hemisphere (Alpine Station). OHP is equipped with the complete set of NDSC instruments, including a stratospheric aerosol lidar [Chazette et al., 1995].

The stratospheric aerosol lidar is a 532 nm backscatter lidar, without depolarization, including a Raman N<sub>2</sub> channel. The instrument has operated on a routine basis since March 1991 although observations exist sporadically since 1986. Clear-sky weather conditions, which prevail mostly at OHP, allow for high frequency lidar operations. The lidar system, except the perpendicular polarization detection and the inversion methodology, are similar to those described below for the Dumont d'Urville lidar. The atmospheric density profiles are derived from daily meteorological radiosondes from Nîmes (about 150 km west of OHP). Daily integrated aerosol backscatter values are obtained between the tropopause and 30 km, with an uncertainty of 10 to 30 %, depending on the aerosol loading.

#### *Hampton – Northern Middle Latitude*

Routine ground-based lidar measurements have been taken at Hampton, Virginia, U.S.A. (37.1°N, 76.3°W) since May 1974 [Fuller et al., 1988; Woods et al., 1994; Osborn et al., 1995]. The instrument consists of a ruby laser that nominally emits 1 joule per pulse at a wavelength of 694 nm at a repetition rate of 0.15 Hz and a 122-cm (48 inch) Cassegrain telescope (field of view 4.0 mrad). The data are collected at 15-m vertical resolution but are software averaged to a 150-m vertical resolution before retrieving and archiving aerosol backscatter and scattering ratio. Splitting of the optical return signal between 3 photomultiplier tubes in the receiver (1 %, 9 %, and 90 %) enables accurate measurements over a large dynamic range. Although there have been incremental improvements in the system, the fundamental operating wavelength and measurement principles have not changed since the 1970s.

Measurements are obtained weekly, weather permitting. Molecular density is calculated from temperature-pressure profiles obtained from the radiosonde station at Wallops Island (120 km northeast of the lidar system). The retrieval procedure for aerosol optical parameters relies on an iterative method. For this mid-latitude station, the integration interval for integrated backscatter is from the tropopause to 30 km. Errors range from 15 to 50 % under low (background) stratospheric loading conditions, decreasing to 5 % for measurements following large eruptions.

#### *Mauna Loa – Northern Tropic*

In Mauna Loa, Hawaii (19.54°N, 155.58°W), lidar observations began in 1974, with a main focus on the stratospheric aerosol [DeFoor and Robinson, 1987; DeFoor et al., 1992; Barnes and Hofmann, 1997; 2001]. The initial system used a ruby laser, emitting at 694 nm. In 1994, a new lidar was built using a Nd:YAG laser operating at 30 Hz, measuring backscatter

at both the 532 nm harmonic and the 1064 nm fundamental. Backscattered light is received by a 61 cm telescope, with an altitude resolution of 300 m (for both systems). Mauna Loa is part of the tropical primary site of the NDSC (Hawaii Station).

As in Garmisch, for data continuity, the 532 nm data are converted to 694 nm to be easily compared with the early measurements. Errors in the integrated backscatter range from 15 % to more than 30 % for the ruby measurements, depending on aerosol load. These errors are reduced to approximately 6 % for the 532 nm measurements. Since the station is located in the tropics, tropopause fluctuations are minor. Thus, the altitude interval for backscatter calculations can be fixed: in this case, 15.8 to 33 km. Molecular density was obtained from a model for the Ruby lidar analysis and from the nearest radiosonde site (Hilo, HI) for the Nd:YAG lidar. There was an overlapping period of about a year (40 observations) during which the ruby lidar backscatter and the Nd:YAG lidar backscatter at both wavelengths were measured. The average absolute backscatter of the ruby lidar agreed to within 2 % of the Nd:YAG backscatter interpolated from the two wavelengths.

### *São José dos Campos – Southern Tropic*

A sodium lidar operating at 589 nm has been used since 1972 at São José dos Campos (23.12°S, 45.51°W), Brazil, for monitoring the vertical distribution of stratospheric aerosols [Clemesha and Simonich, 1978; Simonich and Clemesha, 1997]. Most of the measurements were made as an offshoot of work on atmospheric sodium. The receiving telescope of the lidar was improved and the electronics were recently modified to measure the Doppler temperature of the sodium atoms and Raman scattering from the stratosphere. However, the wavelength used for the measurements has not changed since the start of operations. Early data, up to about 1980, had a height resolution of 2 km, subsequent measurements have a resolution of either 1 km or 250 m.

The aerosol profiles are determined by fitting the lidar backscatter profiles to an atmospheric model at altitudes above 30 km. A single model atmosphere is used for all seasons because the seasonal variation in the atmospheric density profile is small at tropical latitudes. Molecular density profiles are obtained from a standard atmosphere. Because the main purpose of the lidar measurements has normally been to study the 80–110 km region, the signal is sometimes saturated in the lower stratosphere. For this reason the lower limit of the scattering ratio profiles varies between 10 and 20 km. For most monthly averages, however, this limit is less than 15 km. Hence, monthly averages of integrated aerosol backscatter are obtained between 17 and 35 km. Since the site is located in the tropics, the tropopause is high and its fluctuations are minor. Error estimates on the integrated profiles are 5 %.

### *Dumont d'Urville – Antarctica*

The lidar experiment in Dumont d'Urville (66.67°S, 140.01°E) is a French-Italian cooperation that has provided stratospheric aerosol and PSC optical parameter profiles since 1989. Dumont d'Urville is the French Antarctic Station, part of the Antarctic NDSC primary station. The present set of instruments includes a stratospheric aerosol and PSC lidar.

The 532 nm lidar, with depolarization, has operated routinely since June 1989. The frequency doubled Nd:YAG laser emits 450 mJ at a 10 Hz repetition rate. The backscatter signal is collected on an 80 cm diameter Cassegrain telescope and split into two components polarized respectively parallel and perpendicular to the laser emission. Both components are detected by photomultipliers, gain switched to prevent saturation by the stronger returns from

the lower altitudes. The signals are then time resolved with a 30 m vertical resolution and averaged over 5 min. The range and background corrected signal is inverted using the Klett method. The quantities derived from the combined Mie and Rayleigh components of the lidar signal include backscatter ratio and depolarization ratio. The atmospheric density profiles are derived from local daily meteorological radiosondes. Daily integrated aerosol backscatter values are obtained between the tropopause and 28 km, with uncertainties between 15 and 40 %, depending on stratospheric particle loading [David et al., 1998].

**Table 3.2: List of various aerosol lidars which have run or are still running, from northern polar to southern polar latitudes, together with their location, time frame and investigators' names. In blue are the active lidar stations that provide almost continuous long-term series.**

<b>Aerosol Lidar</b>	<b>Location</b>	<b>Time Frame</b>	<b><math>\lambda</math></b>	<b>PI</b>
Eureka (NDSC)	80.05°N - 86.42°W	February 1993 → 2002	1064 nm 532 nm	T. Nagai O. Uchino
<b>Ny-Alesund (NDSC)</b>	<b>78.92°N – 11.93°E</b>	<b>Winter 1991 → now</b>	<b>532 nm</b>	<b>R. Neuber, M. Müller</b>
Thule (NDSC)	76.53°N - 68.74°W	November 1990 → now	532 nm	G. Fiocco
Andoya (NDSC compl.)	69.3°N - 16.00°E	1995 → now	532 nm	A. Hauchecorne
<b>Garmisch-Partenkirchen (NDSC)</b>	<b>47.48°N - 11.06°E</b>	<b>1976 → now</b>	<b>694 nm 532 nm</b>	<b>H. Jäger, T. Trickl</b>
<b>Obs. de Haute-Provence (NDSC)</b>	<b>43.94°N - 5.71°E</b>	<b>June 1991 → now</b>	<b>532 nm</b>	<b>C. David, P. Keckhut</b>
Toronto (NDSC compl.)	43.66°N - 79.4°W	late 1989 → April 2001	532 nm	S. Pal, A. Carswell
Suwon (NDSC compl.)	37.2°N - 127.6°E	November 1995 → now	355 nm	C. H. Lee
<b>Hampton</b>	<b>37.1°N – 76. 3°W</b>	<b>May 1974 → now</b>	<b>694 nm</b>	<b>C. Hostetler, P. Lucker</b>
<b>Table Mountain (NDSC compl.)</b>	<b>34.4°N – 117.7°W</b>	<b>February 1988 → now</b>	<b>532 nm</b>	<b>S. McDermid, T. Leblanc</b>
<b>Mauna Loa (NDSC)</b>	<b>19.54°N - 155.58°W</b>	<b>1974 → now July 1993 → now</b>	<b>694 nm 532 nm</b>	<b>J. Barnes, S. McDermid, T. Leblanc</b>
<b>Saõ José dos Campos</b>	<b>23.2°S – 45.9°W</b>	<b>March 1972 → now</b>	<b>589 nm</b>	<b>D. Simonich</b>
Lauder (NDSC)	45.04°S - 169.68°E	1994 → 1997 1993 → 1999	532 nm	L. Stefanutti T. Nagui
<b>Dumont d'Urville (NDSC)</b>	<b>66.67°S - 140.01°E</b>	<b>March 1989 → now</b>	<b>532 nm</b>	<b>G. Di Donfranceso, C. David</b>
<b>McMurdo (NDSC)</b>	<b>77.9°S – 166.76°E</b>	<b>1990 → now</b>	<b>532 nm</b>	<b>M. Snells</b>

### *McMurdo Station - Antarctica*

The lidar experiment at McMurdo Station (77.85°S, 166.67°E), an Italian-American cooperation, has operated routinely since August 1990, with measurements including the early winter beginning in 1994 [Adriani et al., 1995, 2004]. McMurdo, the American Antarctic station, is one of the Antarctic NDSC primary stations. The frequency-doubled Nd:YAG laser emits a 532 nm polarized signal at 150 mJ and 10 Hz. The backscattered signal is collected with a 40 cm diameter Cassegrain telescope, split into parallel and perpendicular polarizations, and detected with photomultiplier tubes. A mechanical chopper blocks the strong lower altitude signal. The signals are time resolved with a 30 m vertical resolution and averaged over 5 min. The range and background-corrected signal is inverted using the Klett method. The quantities derived from the combined Mie and Rayleigh components of the lidar signal in-

clude backscatter ratio and depolarization ratio. Atmospheric density profiles are derived from local daily meteorological radiosondes. Daily integrated aerosol backscatter coefficients are obtained between the tropopause and 28 km, with uncertainties between 15 and 40 %, depending on stratospheric particle loading [David et al., 1998, Adriani et al., 2004]. In 2004 the lidar system was replaced with a Nd:YAG laser emitting at 1064 nm (100 mJ) and 532 nm (190 mJ), with a 10 Hz repetition rate. The new receiver, a 36.5 cm diameter Schmidt Cassegrain telescope coupled to 5 detectors, is operated in photon counting mode. Three photomultipliers detect at 532 nm parallel polarized light (low and high altitude) and perpendicular polarized light. A fourth photomultiplier tube detects 607.3 nm Raman scattering of 532 nm by molecular nitrogen, and serves for calibration purposes. The fifth detector, an avalanche photodiode, detects the 1064 nm scattering. The 532 to 1064 nm scattering ratio might provide information on aerosol particle size.

### 3.5 Localized Short-Term Measurements

#### 3.5.1 The Aircraft-Borne LaRC Aerosol Lidar

Between July 1982 and February 1984, NASA Langley Research Center (LaRC) deployed an airborne lidar system aboard an Electra aircraft for five missions that reached as far north as 76°N and as far south as 56°S (summarized in Table 3.3). The system consisted of a ruby laser nominally emitting 1 J/pulse at 0.5 Hz at a wavelength of 694.3 nm and a 35.6 cm Cassegrainian-configured receiving telescope. Two photomultipliers, electronically switched on at specific times after the laser firing, are used to enhance dynamic range. The transmitted output divergence is 1.0 mrad and the receiver field of view is 0.2 mrad. Two 40.6 cm quartz windows separated by 1 m were used in the top of the aircraft fuselage. One window was used for the laser transmitter and the other for the receiver. The signal becomes usable at 3 to 4 km above the aircraft flight altitude. A detailed error analysis for this system is described in Russell et al. [1979]. Details of the flight paths and data analysis are available in a series of five NASA Reference Publications by McCormick and Osborn [1985a, 1985b, 1986a, 1986b, and 1987] and summarized in McCormick et al. [1984]. Unfortunately, the digital records of these missions are no longer available and only the tabulated data in the Reference Publications still exist. For the purposes of this report only 3 profiles close to the equator have been included in the analysis though clearly a more ambitious use of this data set would be desirable. Currently, the entire data is in the process of being recovered from paper and it will eventually be archived at the NASA Langley Research Center Atmospheric Science Data Center (<http://eosweb.larc.nasa.gov/>).

**Table 3.3: NASA Langley Airborne Lidar System Flights between 1982 and 1984.**

<b>Dates</b>	<b>Latitude Range</b>
July 1982	42°N to 12°N
October-November 1982	46°N to 46°S
January-February 1983	27°N to 76°N
May 1983	72°N to 56°S
January 1984	38°N to 77°N

The more recently developed NASA LaRC Aerosol Lidar measures profiles of aerosol and/or cloud backscatter at 532 and 1064 nm and aerosol/cloud depolarization at 532 nm. This lidar is a piggy-back instrument on NASA Goddard Space Flight Center's Airborne Raman Ozone,

Temperature, and Aerosol Lidar (AROTAL) lidar. The light source for the aerosol measurements is a Continuum 9050 Nd:YAG laser operating at 50 shots per second. The laser nominally transmits 475 mJ at 1064 nm, 300 mJ at 532 nm, and 225 mJ at 355 nm. AROTAL also employs an excimer laser transmitting at 308 nm and uses the molecular and Raman backscatter from the 355 and 308 beams to measure ozone and temperature. Backscattered light at all wavelengths is collected by a 400 mm diameter Newtonian telescope with a selectable field stop. Directly behind the field stop is a rotating shutter wheel which blocks the near-range (0-4 km) backscatter from the receiver to eliminate the distortions in the relatively weak far-range signals due to transients induced by the very strong near-range signals. In the aft optics assembly following the telescope and field stop, the UV signals are separated from the 532 and 1064 nm signals by a dichroic beam splitter. The UV signals are directed to the AROTAL receiver assembly and the 532 and 1064 nm signals are directed to the LaRC Aerosol Lidar receiver assembly. The 532 and 1064 nm signals are separated by a dichroic beam splitter and the 532 nm signal is further separated into orthogonal polarization components using a polarizing beam cube. A computer-controlled half-wave plate in front of the polarizing beam cube is rotated so that the polarization of the 532 nm signal is measured in components that are parallel and perpendicular to the polarization of the transmitted laser pulse. The signals at both wavelengths and both 532 nm polarizations are transmitted to detectors at the Aerosol Lidar data acquisition rack via fiber optic cables. Each optical signal, the 1064 nm total backscatter and the 532 nm parallel and perpendicularly polarized backscatter, is further split between two detectors, with 10% going to one detector and 90% to the other, in order to more accurately measure the signals over their full dynamic range. In addition to the main channels described above, a “mini-receiver” with a 75 mm aperture measures the 532 and 1064 nm backscatter in the 1-4 km range (i.e., corresponding to that part of the range blocked by the chopper in the main receiver). The 532-nm returns are measured with photo-multiplier tubes and the 1064 nm returns are measured with avalanche photo-diodes. Because of the high optical signal levels, all data are acquired in analog mode, using 12-bit analog-to-digital converters. The instrument operates under both daytime and nighttime lighting conditions, with some degradation in data quality during the daytime due to noise from solar background light.

The signals measured by the instrument are composed of backscatter from both air molecules and aerosol/cloud particles. The aerosol/cloud component of the signal is estimated using density profiles derived from assimilation model results using the technique of Russell et al. [1979]. Data products retrieved from the measurements include: total scattering ratio at 532 nm, total scattering ratio at 1064 nm, aerosol backscatter coefficient at 532 nm, aerosol backscatter coefficient at 1064 nm and aerosol depolarization ratio at 532 nm.

The LaRC Aerosol Lidar participated in the SAGE III and Ozone Loss Validation Experiment (SOLVE) campaign, conducted in the winter of 1999-2000, and the SOLVE-II campaign, conducted in January 2003. For the SOLVE mission, 22 flights were conducted over the course of three deployments, and for the SOLVE-II campaign, 11 flights were conducted over the course of a single deployment. Archived products from the LaRC Aerosol Lidar were generally produced over an altitude range extending from approximately 4 km to 25 km above the aircraft for SOLVE and 1 km to 25 km above the aircraft for SOLVE-II. The difference in coverage was due to the fact that the mini-receiver which captures the near-range signal were not yet installed for the SOLVE mission. Data are acquired at sampling resolutions of 15 m vertical and 500 m horizontal (2 s integration). The archived products are averaged to lower resolutions, generally 75 m vertically and 8 km horizontally, although the data may be averaged to higher resolutions as required by the application.

### 3.5.2 The Airborne DLR OLEX Lidar

The four wavelength aerosol-ozone lidar (OLEX) of the DLR can be operated in upward and downward looking modes. It makes use of a flashlamp-pumped Nd:YAG laser with a fundamental wavelength of 1064 nm. Frequency doubling and tripling provides simultaneous output at 532 nm and 355 nm. The instrument emits the laser beams in an off axis mode via an extra window in the aircraft fuselage. Complete overlap of the laser beams and the receiver FOV is achieved after a distance of 1-1.5 km. The receiver is a 35 cm Cassegrain telescope with 1 mrad field of view. Narrow band filters are positioned in front of the detectors to minimize the contributions of the atmospheric background illumination and the surface. The received 532 nm signal is split into two perpendicularly polarized portions which allow one to calculate the depolarization of the light.

With a repetition rate of 10 Hz and a typical aircraft speed of 150 m/s the raw data resolution is 15 m horizontally. Vertically the 10 MHz analog-to-digital converter (ADC) sampling rate results in a resolution of 15 m. However, depending on the specific demand, a trade-off between signal noise and spatial resolution is performed. In order to qualitatively investigate small scale structures in an inhomogeneous environment (e.g. for comparison of cloud boundaries obtained from ground based radar and airborne lidar) only a few shots (< 1 s) are averaged, degrading the horizontal resolution to about 100 m. For the derivation of quantitative optical parameters like optical depth or the multiple scattering contribution the signal is typically averaged over 10-20 s and slightly smoothed vertically which leads to a resolution of 1-3 km horizontally and 30 m vertically.

The attenuation of the laser beam in the atmosphere is treated by employing a numerical Klett-type inversion of the lidar equation in which an extinction/backscatter coefficient ratio (lidar ratio) and a starting value at some distance from the receiver have to be assumed to iteratively derive the profiles. With the inferred lidar ratio the extinction coefficient and its integral, the optical depth, can be estimated from the backscatter signal. The depolarization of the 532 nm signal by the scattering particles contains information about their shape. A volume depolarization of 0.014 (or 1.4 %) occurs if only the asymmetric air molecules contribute to the depolarization. If the sampled volume contains depolarizing (non-spherical, solid) particles, the volume depolarization is between 0.014 and 1 depending on the concentration and shape of the scattering particles. Clouds with *only* spherical (liquid) particles may cause volume depolarization below 1.4 % since they increase only the intensity in the parallel channel.

### 3.5.3 Airborne Particle Counters

#### *NMASS, FCAS and Passive, Near-Isokinetic Inlet*

The University of Denver Focused Cavity Aerosol Spectrometer, FCAS, is a single particle, optical aerosol spectrometer that detects particles in the 90 to 1000 nm diameter range [Jonsson et al., 1995]. Stratospheric aerosol is dominated by sulfuric acid and water. The measured size distributions essentially correspond to those for dry aerosol particles because the sample is heated prior to measurement. Water vapor and temperature measurements made by other investigators are used to determine the ambient size distributions from measured dry distributions. FCAS has been an element of a number of field campaigns (summarized in Table 3.4) that has produced measurements that span, in the Northern Hemisphere, the equator to the pole and 7 km to 21 km in altitude. The ambient integral parameters are available to the public at the NASA ESPO website

([www.espoarchive.nasa.gov](http://www.espoarchive.nasa.gov)).

The response matrix of the FCAS II was determined from numerous calibrations and is used in a Twomey inversion [Markowski, 1988] to determine the measured size distribution from FCAS output. Over the last seven years, the FCAS II has been tested with more than 350 monodisperse aerosols at pressures that covered the range experienced by the instrument in flight. On average, the absolute value of the discrepancy between the particle diameters determined from the FCAS response and that determined from the differential mobility analyzer settings used to obtain the test aerosols is less than 3 % of the diameter. Calibrations for concentration were done using a dual-channel, low-pressure condensation nucleus counter, CNC, and show an uncertainty of around 15 % [Wilson et al., 1983]. The FCAS data provide accurate measurements of stratospheric aerosol surface and volume except from October 1992 through April 1993 when some particles were larger than its upper detection limit due to the eruption of Mt. Pinatubo. Data combining FCAS and FSSP measurements from this period are available from J. C. Wilson at the University of Denver. The FCAS data from 1994 do not meet the standards of accuracy described in this report.

Prior to 1998, knowledge of smaller particles was limited to number concentration and resulted from measurements with a low-pressure condensation nucleus counter. Since 1998, the Nuclei-Mode, Aerosol Size Spectrometer (NMASS) has been flown on 6 missions [Brock et al., 2000]. The NMASS consists of 5 condensation nucleus counters. Each CNC has a different threshold for detecting particles due to different temperature differences between the saturator and condenser. The 50 % detection sizes for the five CNCs are set to approximately 4, 8, 16, 32, 60 nm. These characteristics remain constant with altitude because the NMASS is run at a constant pressure. The full response matrix and the Twomey inversion are used when retrieving size distributions from the CNCs outputs. The combined dry NMASS and FCAS size distributions are archived at the NASA ESPO website.

The passive, near-isokinetic inlet employs two diffusers to slow the sample flow from the true air speed of the aircraft to appropriate instrument speeds [Jonsson et al., 1995]. The inlet is instrumented and the size distribution data are corrected for deviations from isokinetic sampling.

#### *FSSP and MASP*

FSSP (Forward Scattering Spectrometer Probe) and MASP (Multiangle Aerosol Spectrometer Probe) at NCAR (National Center for Atmospheric Research) are two instruments that measure the intensity of light scattered by individual particles that pass through a focused laser beam. The FSSP-300 collects the light that is forward scattered over angles between 4° and 12°. The MASP uses a different light collection geometry and collects light from 30°-60° and 120°-150°. The size of particles (in the radius size range from 0.2 to 20 µm) are derived from both instruments with Mie theory that relates the intensity of light scattering to particle size, refractive index, angle of light collection, and laser wavelength. The number concentration is derived by dividing the number of particles detected by the known volume of the air sampled by each instrument. The surface area and volume is derived from the integrals of the size distributions, weighting the concentration at each size category by either the area or volume of a sphere for that size. This assumes that the particles are spherical.

**Table 3.4: Missions in the NASA ESPO archive with FCAS and CNC or NMASS Data.**

<b>Mission Identifier</b>	<b>Aircraft Identifier (ext)</b>	<b>Year</b>
AASE2	ER2	1991-1992
SPADE	ER2	1993
STRAT	ER2	1995-1996
POLARIS	ER2	1997
WAM	WB57	1998
ACCENT	WB57	1999
SOLVE	ER2, DC8	2000
CRYSTALF	WB57	2002
SOLVE2	DC8	2003
Pre-AVE	WB57	2004

**Table 3.5: Chronological summary of aircraft missions with stratospheric aerosol measurements using the FSSP-300 or the MASP.**

<i>Aircraft Mission</i>	<i>Aircraft</i>	<i>No. of Flights</i>	<i>Dates</i>	<i>Latitude Range</i>	<i>Particle Probe</i>
AASE I	ER-2	18	12/88 – 2/89	30°N – 90°N	FSSP-300
AASE II	ER-2	29	10/91 – 3/92	22°N – 90°N	FSSP-300
SPADE	ER-2	12	10/92 – 5/93	15°N – 60°N	FSSP-300
APE-POLECAT	Geophysica	9	12/96 – 1/97	42°N – 78°N	FSSP-300
ASHOE/MAESA	ER-2	25	3/94 – 11/94	70°S – 60°N	MASP
POLARIS	ER-2	22	4/97 – 9/97	3°S – 90°N	MASP
WAM	WB-57F	4	5/98	9°N – 45°N	MASP
APE-THESEO	Geophysica	4	2/99 – 3/99	42°N – 9°S	FSSP-300
ACCENT	WB-57F	6	9/99	5°N – 40°N	MASP
SOLVE I	ER-2	14	1/00 – 3/00	35°N – 90°N	MASP
EUPLEX/Envisat	Geophysica	18	1/03 – 3/03	42°N – 78°N	FSSP-300

In situ measurements were made with these optical particle spectrometers on three airborne platforms, the NASA ER-2 and WB-57F from 1989 to the present day, and the Russian Geophysica from 1996 to present. The measurements on the ER-2 were from 136 flights carried out during six missions, on the WB-57F they were from 10 flights made during two missions, and on the Geophysica they come from 31 flights during 3 missions. Table 3.5 lists the project information.

The operating principles, measurement limitations and uncertainties of the FSSP-300 are discussed by Baumgardner et al. [1992]. The primary uncertainty is in the determination of particle size as a result of the dependency of light scattering on refractive index that is sensitive to composition. As the composition is generally not known with any great accuracy, the Mie function can vary from 5-50 %, depending on size and composition. Thus, the estimated, average uncertainty in sizing from the FSSP-300 is approximately 20 % over the 0.2-20  $\mu\text{m}$  size range of this instrument. The uncertainty in measuring concentration,  $\sim 15$  %, is primarily a result of how well the sample volume can be determined. These uncertainties in concentration and size are propagated when calculating surface area and volume, since these depend on the square and cube of the diameter, respectively. The estimated accuracies in derived surface area and volume are 25 % and 35 %, respectively.

The operating principles of the MASP are discussed by Baumgardner et al. [1995]. The uncertainties are similar to the FSSP-300 since the measurement principle is similar. The major difference in the two instruments is the optical geometry. Additional information about the particle composition can be derived from the MASP since two intensity measurements are made from each particle, a forward scattering component and a backward scattering component. The ratio between the forward and backward scattering components is a function of size and refractive index. This allows an estimate of the particle refractive index and hence a lowering of the uncertainties in sizing [Baumgardner et al., 1996].

### 3.5.4 Balloon-borne Backscattersonde

The backscattersonde, developed between 1987 and 1989, measures the locally backscattered light at two wavelengths in the red and blue range. The measurements are representative of the ambient aerosol scattering properties within about 10 m of the instrument. The sampled volume is on the order of 1 m<sup>3</sup>. The instrument, designed to be carried about 50 m below a balloon, also measures ambient pressure and temperature and is sensitive to both tropospheric and stratospheric aerosol. The light source is a quasi-collimated beam from a 10 J xenon flash lamp. The returned signal is detected with two silicon photodiodes using filters to limit the wavelengths sensed. The distribution of wavelengths and backscatter angles associated with the backscattersonde is taken into account in modeling the instrument response. The results of the modeling show only a small difference between the response for 180 degree backscatter and the backscattersonde for stratospheric aerosols. The uncertainty associated with the distribution of wavelengths passing each filter can be essentially eliminated for natural aerosols by selecting 921 and 495 nm as the effective wavelengths. Changes in lamp intensity from flash to flash and over the course of a flight are accounted for with two separate reference photometers which are used to correct the measured backscatter signals in each color channel.

Calibrating the instrument requires, similar to a lidar, determining the Rayleigh (molecular scattering) signal at a known pressure and temperature. In principle this can be done in aerosol free air; however, at the surface, it is not possible to achieve completely aerosol free air without introducing additional complications such as scattering from the walls of an aerosol free chamber. Thus, somewhat indirect methods have been developed. One method consists of maintaining a ground standard (consisting of 4 separate instruments) against which all backscattersondes are compared prior to flight. The Rayleigh signal can then be determined from the flight instrument if it encounters an aerosol free region at high altitude. In practice this has only been achieved in the winter polar regions. There, on a number of flights, the instrument response has apparently approached the theoretical Rayleigh limit above 20 km. The results from these flights can then be used to calibrate the ground standard and in effect all flights which have been compared with the ground standard. In 1999, another more reliable method of calibration was developed which consisted of comparing a “mini-backscattersonde” that could be calibrated in an aerosol free chamber with the flight backscattersonde (Rosen, 2000, unpublished manuscript). This resulted in a slight change in the absolute calibration of all backscattersonde data. All of the soundings reported to the NDSC reflect the 1999 absolute calibration effort.

The accuracy of measured backscatter is nominally 1-3%, with an effective resolution of .5-1% at altitudes below 20 km. Above 20 km statistical fluctuations in backscatter due to low signal become noticeable and may dominate other uncertainties at the highest altitudes. These fluctuations can be reduced by averaging with a corresponding loss in altitude resolution. To represent an aerosol measurement the backscattered signal is divided by the theoretical molecular scattering determined by ambient pressure and temperature and the ground calibra-

tion. This gives the backscattering ratio = (aerosol scattering + molecular scattering)/molecular scattering.

A more complete description of the backscattersonde, its calibration, and the comparison with other instruments can be found in Rosen and Kjome [1991b] and Rosen [2000, unpublished manuscript]. Methodologies and formulas for converting backscattersonde measurements to equivalent measurements from lidar, satellite extinction and mass mixing ratios can be found in Rosen [2000, unpublished manuscript].

The first backscattersonde measurements began in Laramie, Wyoming, in May 1989. Since then the instrument has been flown in the Arctic [e.g. Rosen et al., 1989; 1994a; Larsen et al., 1996], in the Antarctic [Rosen et al., 1991; 1993], in volcanic aerosol [Rosen et al., 1992; 1994b], in the mid latitudes [McKenzie et al., 1994], in the tropics [Rosen et al., 2004], and has been used to analyze tropospheric aerosol profiles [Rosen et al., 1997; 2000]. Table 3.6 summarizes the backscattersonde flight history.

**Table 3.6: Flight history, as of March 2005, of the backscattersonde. These data are publicly available on the NDSC web site, <http://www.ndsc.ws/>.**

<i>Location</i>	<i>Latitude</i>	<i>Longitude</i>	<i>Altitude</i>	<i>Number of flights</i>	<i>Dates</i>
Laramie WY	41.3 N	105.6 W	2160	93	5/89- 9/00
Lauder New Zealand	45.0 S	169.6 E	370	77	2/92- 3/00
Natal Brazil	6.1 S	35.3 W	50	42	11/95-10/04
Cuiaba Brazil	15.0 S	56.0 W	225	3	8/9/95
Mildura Australia	34.2 S	142.1 E	52	4	9/10/98
South Pole Station	90.0 S	0.0 E	2835	11	winters 90&91
Table Mountain CA	34.4 N	117.7 W	2260	4	Mar-97
Boulder CO	40.0 N	105.1 W	1743	3	7/89- 5/90
Alamogordo NM	33.3 N	105.0 W	1280	2	Jun-90
Vanscoy Canada	52.1 N	106.6 W	50	4	8/91- 9/00
Air sur l'Adour France	43.7 N	00.3 W	79	2	Mar-94
Gap France	44.5 N	06.0 E	550	1	Jun-93
Rylsk Russia	51.6 N	34.7 W	200	5	8/89-10,92
Moscow Russia	56.0 N	41.0 E	190	2	Jun-94
Kiruna Sweden	67.9 N	21.1 E	327	17	11/91- 1/00
Sodankyla Finland	67.4 N	26.6 E	179	54	9/94- 3/05
Thule Greenland	76.5 N	68.8 W	60	32	1/92-12/97
Scorebysund Greenland	70.5 N	21.5 W	60	5	10/94- 2/96
Sondre Stromfjord	67.0 N	50.9 W	50	2	3/95- 1/96
Ny Alesund	78.9 N	11.9 E	10	16	1/96- 2/05
Heiss Is. Russia	80.6 N	58.1 E	10	12	1/89- 3/92
Alert NWT Canada	82.5 N	62.3 W	66	35	1/89- 1/93
Resolute Canada	74.2 N	95.0 W	40	1	Oct-91
Arkhangel'sk Russia	64.6 N	40.5 E	4	3	1/93- 1/94
Dixon Is. Russia	73.5 N	80.2 E	42	5	1/91- 3/92
Salekhard Russia	66.5 N	67.5 E	160	2	2/99- 1/00
Yakutsk Russia	62.0 N	130.9 E	106	10	1/95- 3/98